



Impact of nodular structure in characterization of three thin film composite membranes made from 1,2-benzisothiazol-3(2H)-one, sodium salt

A. Adeniyi, M.S. Onyango, M.F. Bopape

Department of Chemical, Metallurgical and Materials Engineering, Tshwane University of Technology (TUT), Private Bag X680, Pretoria 0001, South Africa.

Received 07 May 2019,
Revised 14 May 2019,
Accepted 14 May 2019

Keywords

- ✓ Nodular structure,
- ✓ Membrane,
- ✓ characterization,
- ✓ Polymerization,
- ✓ Water treatment.

adeniyia@tut.ac.za ;
Phone: +27789240238

Abstract

This study identifies nodular structure as a major property that affects other properties of membranes and consequently may affect their performances in water treatment. Three commercially available membranes made 1,2-benzisothiazol-3(2H)-one, sodium salt were characterized using SEM-EDX, AFM, FTIR, XRD, TGA and sensile drop measurement. EDX and FTIR revealed the similarity of the polymer base of the three membranes, however, XRD identified that different additives might have been used during the fabrication process. SEM and AFM analysis confirmed the presence of nodular structure at different magnitude on each membrane and differentiated their properties. Fourier transform infrared analysis showed the functional groups at 1650 cm⁻¹ which indicated that polymerization took place during the fabrication of these membranes. The degree of polymerization might have been varied to result in different nodule sizes. In all the roughness parameters increase with increase in the nodule sizes, and the membrane with biggest nodule sizes demonstrated highest value of contact angle.

1. Introduction

Actual separation of solutes and permeation of water occur on the surface skin of the thin film composite membranes. Basically, the characterization of the surface morphological structure is the first important step for the fundamental understanding of the membrane performance [1]. Key membrane properties affecting rejection that were identified in the literature include molecular weight cut-off, pore size, surface charge (measured as zeta potential), hydrophobicity/hydrophilicity (measured as contact angle), and surface morphology (measured as roughness) [2-3]. The performance of the membrane depends largely on the physical or molecular structure of the active layer and there is evidence that nodular structure has some relationship with membrane performance [4]. Some of the method used to characterize membranes include Scan Electron Microscopy-Energy Dispersive X-Rays (SEM-EDX) [5-6] which reveals the surface morphology and elemental composition. Atomic Force Microscopy (AFM) is a high-resolution imaging technique that can be used for image capturing and analysis for both electrically conductive and non-conductive materials [7-8]. The phase composition and functional group are determined using X-Ray Diffraction (XRD) [9] and Fourier Transform Infrared Spectroscopy (FTIR) [10] respectively. Thermal Gravimetric Analysis (TGA) is a method used to measure the thermal stability of material. This is applicable for membrane analysis so that the stability of the membrane at various temperature can be established [11]. Measurement of contact angles of a material is the primary data needed to study the wettability of the material. The data is an indication of the degree of wetting when a solid and liquid contact one another and interact. Contact angle less than 90° is an indication of high wettability while contact angle greater than 90° corresponds to low wettability [12].

Properties such as nodular structure, surface roughness, hydrophilicity, and thermal stability were investigated for the purpose of comparison in order to identify the unique properties that will be useful in application to general membrane and membrane process design for water treatment.

2. Material and Methods

2.1 Materials

Three commercially available membranes obtained from Xylem UK were used for this experiment. The membranes investigated were made from the same material. This was to allow for the comparison of the unique properties that will be useful in application to general membrane and membrane process design for water treatment. The material used for the membrane manufacture was 1,2-benzisothiazol-3(2H)-one, sodium salt. They are tubular membranes of about 32cm in length and 1.4cm in diameter. The trade names are AFC40, AFC80 and AFC99. AFC40 is a loose reverse osmosis (NF) membrane while AFC99 and AFC80 are tight reverse Osmosis membranes. The membrane properties given by the manufacturer are listed in Table 1

Table 1: Membrane properties as given by the manufacturer.

Type	Material	pH range	Operating Pressure	Operating Temperature	Retention	Generic specification	Hydrophilicity
AFC99	Polyamide	1.5 - 12	64	80°C	99% NaCl	RO	3
AFC80	Polyamide	1.5 - 10	60	70°C	80% NaCl	RO	4
AFC40	Polyamide	1.5 - 9.5	60	60°C	60% CaCl ₂	NF	4

2.2 Method

The surfaces of the membranes were scanned using Joel Field Emission Electron Microscope JESM-7600F. The virgin membranes were mounted on a double-sided carbon tape and the surfaces were coated with iridium (about 5 nm thickness) in order to make it conductive before SEM analysis. The sample was exposed to the electron beam at an accelerating voltage of 15 KV. EDX data was obtained during SEM measurement. The SEM images were analyzed with the aid of WSxM 5.0 Develop 8.2 software [13] and ImageJ software [14] for surface roughness, percentage porosity, and pore identification.

A non-contact AFM imaging was performed on the three samples of the membranes using an Agilent Technologies PicoPlus-Atomic Force Microscopy Series 5500. The clean sample was cut into small pieces and glued onto a sample holder with an agar tape. The AFM cantilever used was made out of silicon (Nanosensors) with a resonant frequency of ~60 kHz, a nominal spring constant of 7.4 N/m with a typical tip radius of less than 7 nm. The AFM measurements were performed on dry membranes in an air atmosphere with relative humidity of ~ 30%. The images were flattened with order 1 and the RMS (root-mean-squared) value of the roughness was obtained by using the Nanotechnology Research Tool. The roughness and the phase shifts were measured for the 1.0 μm x 1.0 μm and measurements were done five times on the area in order to obtain the root mean square. Fourier transform infrared spectroscopy was performed on the membrane samples using a PerkinElmer Spectrum 100 spectrometer (PerkinElmer, USA) between 500cm⁻¹ and 4000 cm⁻¹ wave number.

The phase identification was carried out using WAXD Pan Analytical Xpert Pro diffractometer. It was done with a Cu K α radiation having a wavelength of 0.15 nm, a voltage of 45 kV, and a current 40 mA.

The TGA was done using PerkinElmer TGA 8000™ Thermogravimetric analyzer. The material was held for 1.0 min at 30.00°C, heated from 30.00°C to 85.00°C at 40.00°C/min. then held for 1.0 min at 85.00°C, heated from 85.00°C to 900.00°C at 40.00°C/min and lastly Cooled from 900.00°C to 85.00°C at 40.00°C/min.

Contact-angle measurements for the membrane were done using Sessile drop water measurement. The equipment used was Dataphysics Contact Angle Instrument (SCA 20, OCA 15EC). This was done by depositing sessile drops of deionized water on the dry surfaces of the membranes at room temperature. Images were captured five seconds after depositing the water drop onto the sample just before the measurement of the contact angles. Eight measurements were taken at different locations of each membrane sample. The average was calculated to obtain the membrane's contact angle.

3. Results and discussion

3.1 Chemical Composition

The elemental composition was characterized using EDX and the results are shown in Table 2. The surface functional group of the active surface was characterized using FTIR analysis and the results are shown in Figure 1. The elemental composition and the functional group composition of the three membranes are similar which shows that the three membranes were made from the same material. The atoms of carbon, oxygen, sodium, and sulphur identified are due to the fact that the membranes were made from 1,2-benzisothiazol-3(2H)-one, sodium salt.

Table 2: Surface atomic composition of the active layer. This shows similar atomic composition because the membranes were fabricated from the same material.

Membrane	Carbon (%)	Oxygen (%)	Sodium (%)	Sulphur (%)
AFC40	75.96	20.90	0.23	2.90
AFC80	75.71	20.28	0.51	3.50
AFC99	74.33	20.34	0.31	5.02

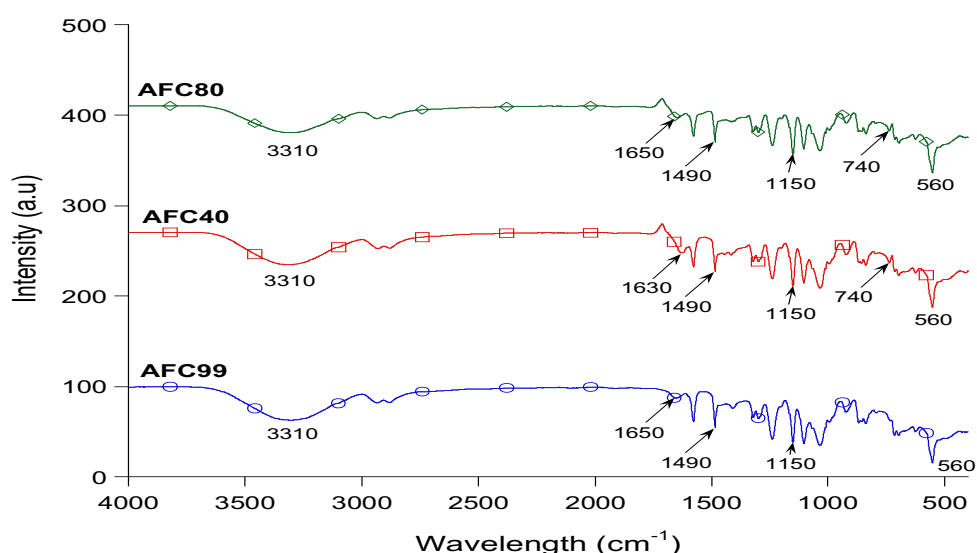


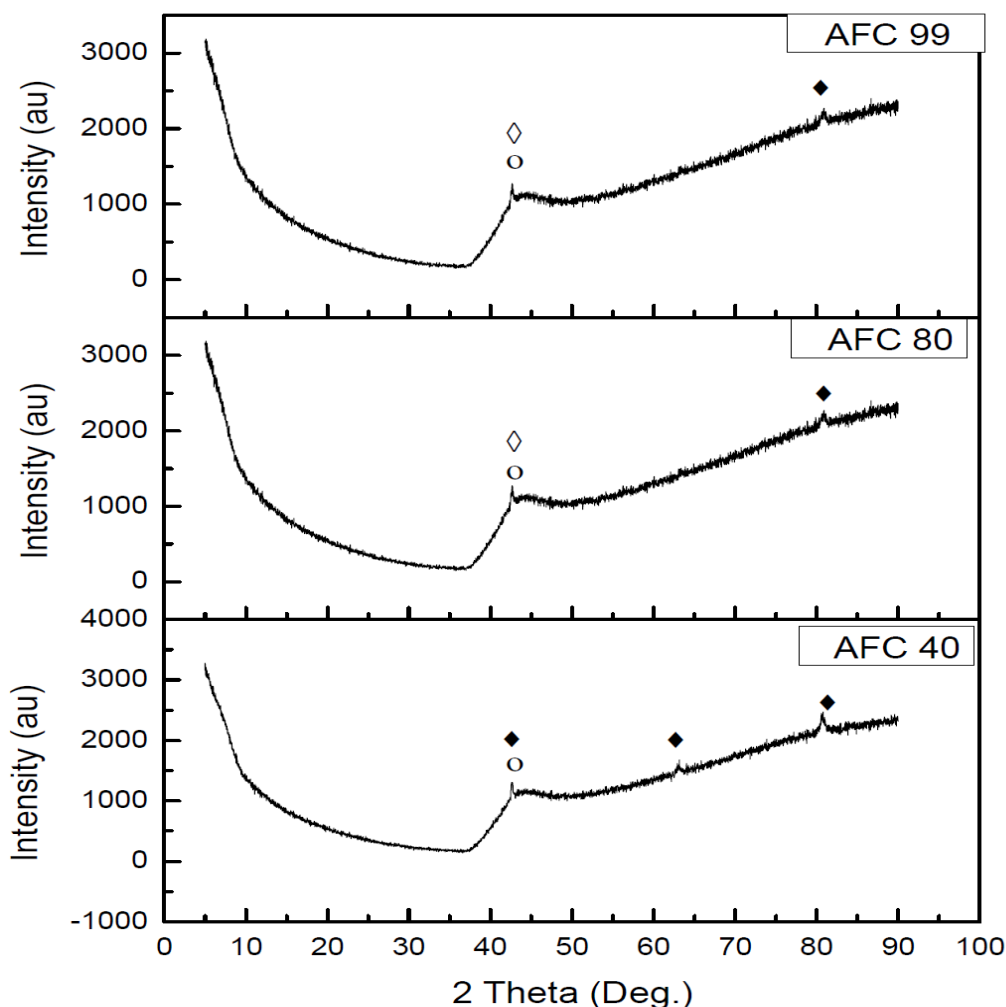
Figure 1: FTIR spectra of AFC40, AFC80 and AFC99 showing a very similar pattern. The presence of polysulfide blend support in the three membranes is shown by the spectra of the membranes having peak of 1150 cm^{-1} . The presence of the strong band at 1650 cm^{-1} is an indication that interfacial polymerization occurred [15].

Phase composition of each of the membranes is shown in Figure 2. All the membranes showed crystalline phases of Sodium hydroxide (NaOH) at 43° and Sodium Hydrogen Sulfamate ($\text{Na}_2\text{H}(\text{N H}_2\text{S O}_3)_3$) (43° and 81°). The phase composition also pointed to the fact that the membranes were made from 1,2-benzisothiazol-3(2H)-one, sodium salt. The pattern for AFC40 is a bit different from that of AFC80 and AFC99, it shows the presence of Sodium Hydrogen Sulfamate at $43^\circ, 64^\circ, 81^\circ$ while both AFC80 and AFC99 shows the presence of sodium sulphate at 43° . This is an indication that although the membranes were made from the same polyamide, there are additives that might have been added to affect the structure of the membranes. Both AFC80 and AFC99 have the same additive while AFC40 has an additive that is different. The presence of sodium hydrogen sulfamate might have contributed to some differences observed in the properties of the membranes. From the manufacturer data, AFC40 is an NF membrane while both AFC80 and AFC99 are reverse osmosis membranes. This means AFC40 is loose and porous while AFC80 and AFC99 are tight membranes.

3.2 Nodular Structure

When considering membrane surface properties, the size of nodules and nodule aggregates are very important. A nodule is a mass of polymer molecule agglomerates that are entangled with each other, that are always found

at the surface of the polymeric membranes [4]. Nodular structures cause “peaks” and “valleys” on the membranes and make the membrane rougher [16]. Rough membranes are known to have more water permeability due to availability of water absorption sites, they are, however, also prone to fouling [17-19]. Nodular structures on the three membranes investigated were studied using AFM and SEM. Data obtained from exposing the virgin materials to infrared radiation (FTIR) were also used to make clarification on the structures obtained from AFM and SEM.



◆ $\text{Na}_2\text{H}(\text{NH}_2\text{SO}_3)_3$ Sodium Hydrogen Sulfamate. ○ NaOH . ◇ $\text{Na}_2\text{S}_2\text{O}_3$ Sodium Sulfate.

Figure 2: X-ray Diffraction showing crystalline phases in AFC40, AFC80 and AFC99. All the membranes showed crystalline phases of Sodium hydroxide (NaOH) at 43° and Sodium Hydrogen Sulfamate ($\text{Na}_2\text{H}(\text{NH}_2\text{SO}_3)_3$) (43° and 81°).

Figure 3 shows the AFM $1\mu\text{m}$ scan of AFC40, AFC80 and AFC99 while the SEM images are shown in Figure 4 for magnification of 30,000. The nodular structure is more pronounced in AFC40 and AFC80 than AFC99. AFC40 and AFC80 show a rough surface with a nodular structure [20]. This suggests that the film might have been formed over polysulfone blend supports [21]. The nodular structure of all the membranes was similar to that observed in a typical membrane made from polyamide that have been fabricated using interfacial polymerization [22].

The surfaces of the membranes progressively smoothen out from AFC40 to AFC99, this can be interpreted in terms of the method of membrane fabrication. The selection of membrane fabrication method is based on the type of polymer and the desired structure of the membrane [3]. This is because the pore characteristics of a membrane are influenced by the molecular characteristic of the polymer and by the method of fabrication [4]. Most commonly used methods of fabrication are phase inversion and interfacial polymerization [23-25]. Other methods include stretching, track etching and electrospinning, however, interfacial polymerization is the most important method for fabrication of thin film composite RO and NF membranes [3, 26].

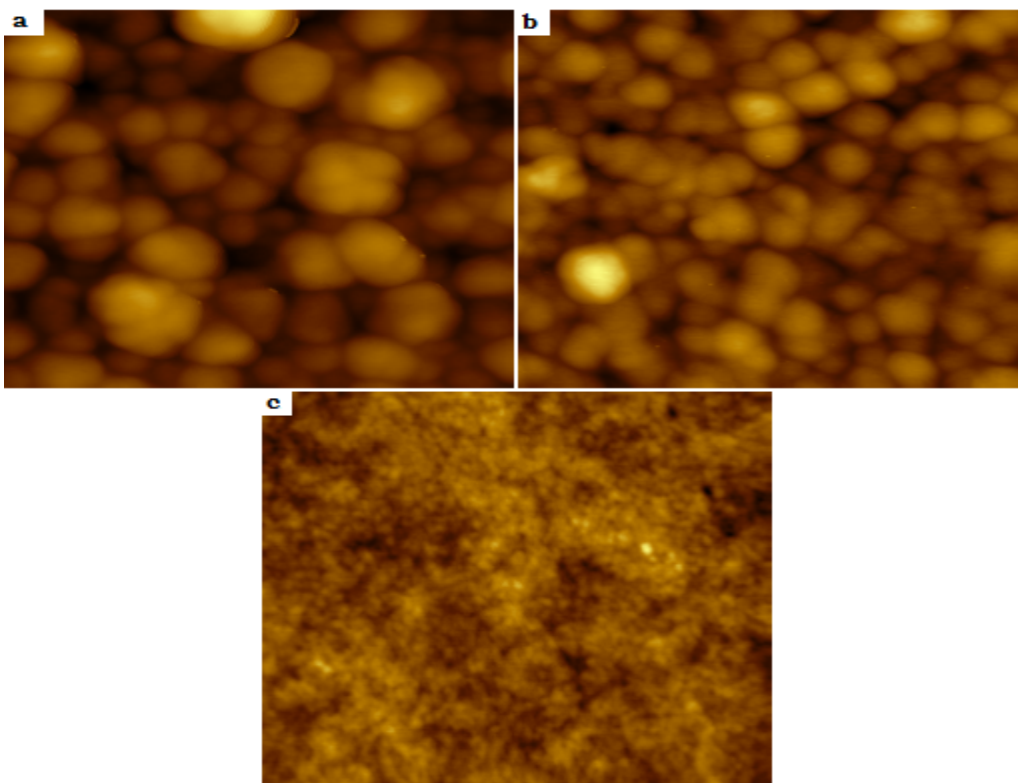


Figure 3: AFM images of AFC40 (a), AFC80 (b), AFC99 (c) at 1 μ m scan. The nodules are more visible and bigger in AFC40 and AFC80

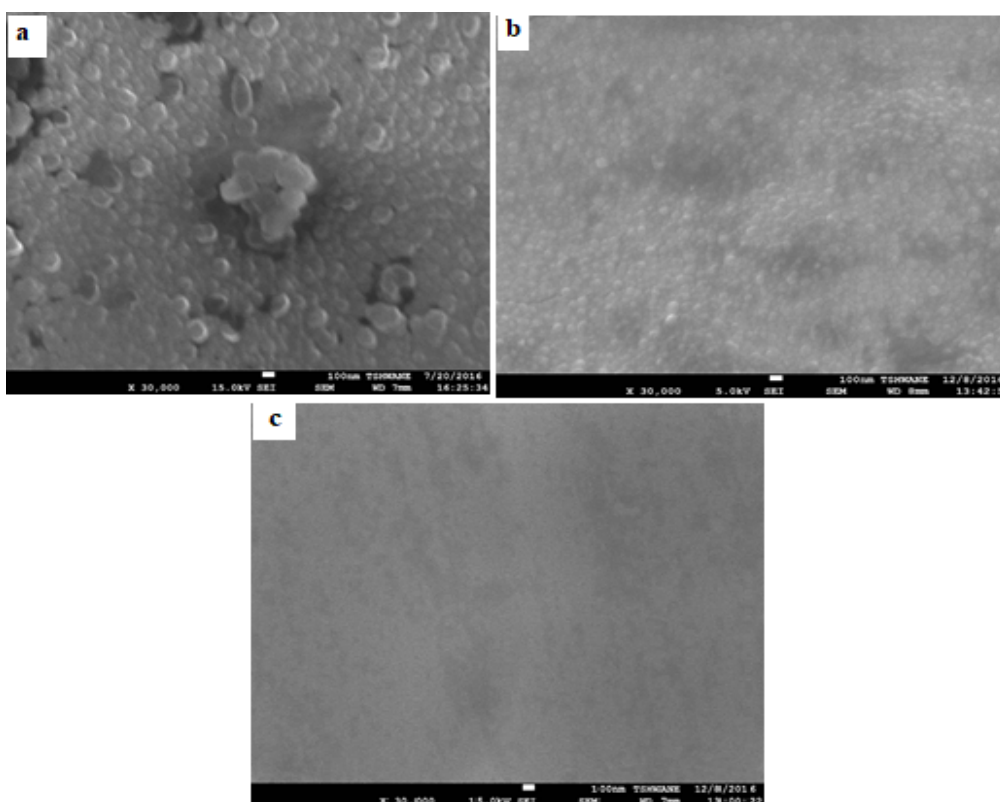


Figure 4: SEM images of AFC40 (a), AFC80 (b), AFC 99(c) at 30,000x. AFC99 appears smooth while the AFC40 and AFC80 shows a rough surface with nodules [15].

If the membranes were manufactured using interfacial polymerization, the progressive invisibility of the nodular structure from AFC40 to AFC99 is an indication that the reaction time during interfacial polymerization increases from AFC40 to AFC99 [27]. For shorter reaction time, the degree of cross-linking is lower, and the

“thin and loose” polyamide skin layer will allow the higher permeation of both water and salt. As the reaction time extends, the thickness and cross-linking degree of the polyamide skin layer will increase, which results in reduced water flux and increased salt rejection. AFC99 appears denser and smoother than the rest of the membranes. These are indication for lower water recovery but higher salt rejection. On the other hand, if the method of manufacture is phase inversion, the degree of undercooling is higher with AFC99 than for both AFC80 and AFC40. This is because the larger the degree of undercooling, the finer the membrane structure [28] and also the smaller the pore size [29].

However, an investigation of the chemical composition using FTIR showed a strong presence of saturated amides group and weak amines group in each of the membranes with equal intensity as indicated by peak at 1650 cm^{-1} for AFC40, AFC80, and AFC99 (Figure 1). The presence of polysulfide blend support in the three membranes is shown by the spectra of the membranes having peak of 1150 cm^{-1} . This peak also indicates a strong presence of acyl and phenyl C-O groups in all the membranes. This is because spectra for sulfones show strong absorption bands at $1160\text{--}1120\text{ cm}^{-1}$ and hydrogen bonding results in absorption near 1125 cm^{-1} [10]. There is strong presence of saturated amides group and weak amines group in each of the membranes with equal intensity as indicated by peak at 1650 cm^{-1} . This means that the membranes were likely manufactured using interfacial polymerization because the presence of the strong band at 1650 cm^{-1} is an indication that interfacial polymerization occurred [27]. The peak results from infrared radiation absorption by C-C stretch aromatic and N-H blends in the active polyamide layer. This is expected, because the membranes are made from 1,2-benzisothiazol-3(2H)-one, sodium salt, a polyamide. There is also the presence of amines group with equal intensity for AFC99 and AFC40 but higher than the intensity of AFC80 (peak at 3310 cm^{-1}). The peaks at 3310 cm^{-1} means the presence of primary sulfonamides in all the membranes which show strong N-H stretching bands at $3300\text{--}3247\text{ cm}^{-1}$ [10]. There is the presence of orthodisubstituted aromatic group in each of the membranes (peak at 740 cm^{-1}) but was not observed in AFC99. This might have contributed to the structure of AFC40 and AFC80 because the presence of substituted groups affects the membrane properties [30]. The peak results from infrared radiation absorption by C-C stretch aromatic and N-H blends in the active polyamide layer.

SEM images of AFC99 shows very low nodular structure and a very smooth surface. The three dimensional images of SEM images using WSxM 5.0 Develop 8.2 and the AFM images shown in Figure 5 reveal that all the membranes actually have nodules. The nodules were further examined using AFM and the nodular sizes calculated. The size of a nodule as revealed by the AFM images was determined from the cross-sectional profiles of the data along a reference line shown in Figure 6. The measurement of nodule diameters shown in the bright sites are nodules and the dark sites are interstitial domains. The nodule diameters were measured using the vertical lines drawn before and after three of the nodules.

The average diameter of the nodules in AFC40 was calculated to be 130nm, while that of AFC80 and AFC99 was 120nm and 50nm respectively.

3.3 Surface roughness

Surface roughness influences the transmembrane transport and fouling potential and is therefore an important parameter in evaluating the performance of the membrane. Interaction of colloidal particles with polymeric membrane surfaces is influenced by membrane surface roughness [31]. Minimization of membrane fouling by colloids can be achieved by choosing membranes with a roughness periodicity preventing penetration of foulants into valleys on the surface [32]. Bowen and Doneva also stated that surface roughness may lead to a difference in adhesion on peaks and in valleys of more than a factor of 20; they suggested that such variations need to be taken into account in mathematical descriptions of membrane processes and in the choice of membranes for a given process [32]. Khulbe et al. stated that the pore size increased as the surface roughness increased [4].

Two of the most quoted parameters for membrane surface topographies are the roughness average (R_{avg}) and the root mean square (RMS) roughness (R_{rms}). The roughness average is the arithmetic mean of the surface height (peaks and valleys) deviations from the mean plane of the image. The RMS roughness is the standard deviation of the pixel height data, that is, the deviation of the peaks and valleys from the mean plane.

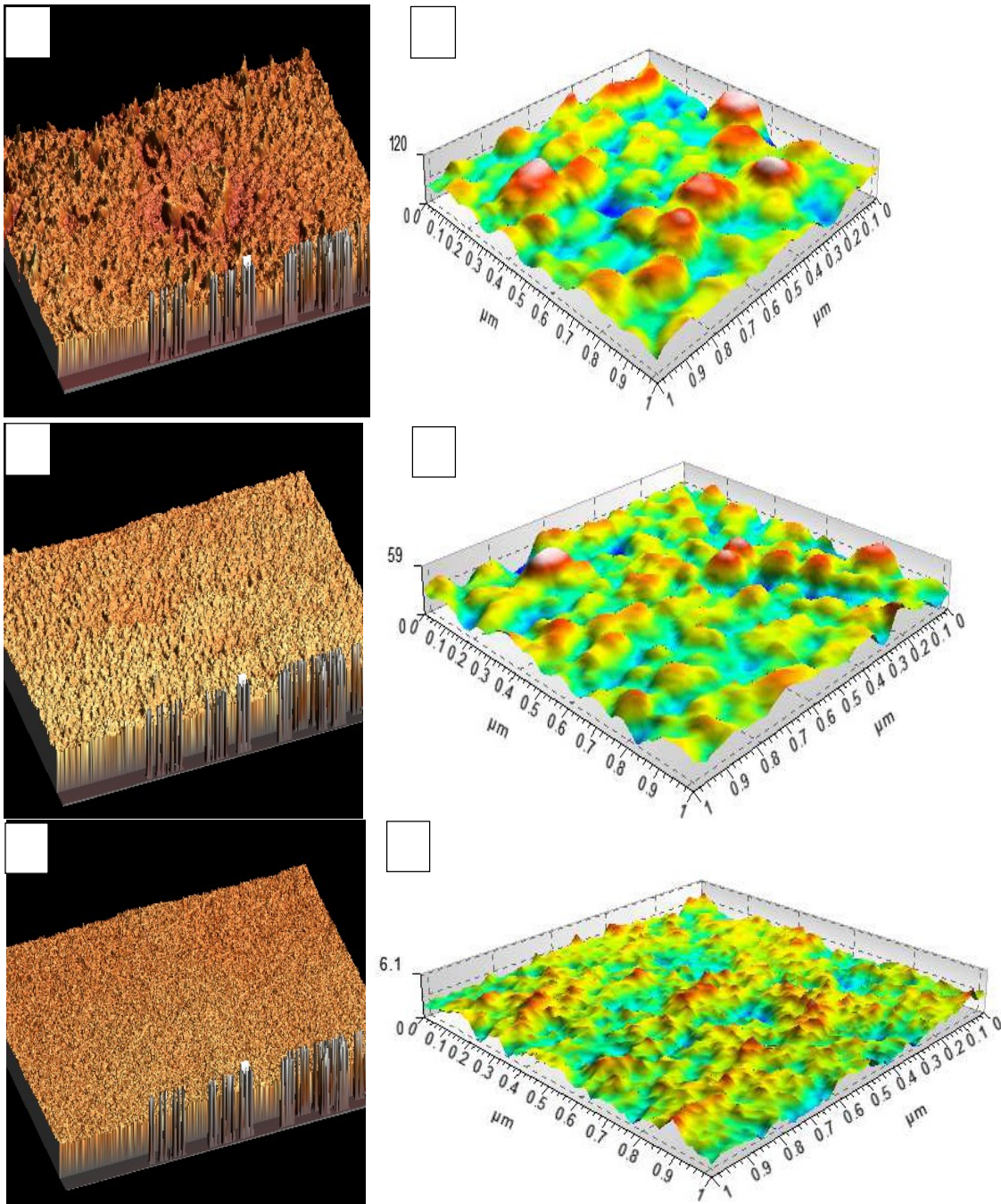


Figure 5: 3D SEM images analysed using WSxM 5.0 Develop 8.2 for AFC40 (A), AFC80 (C) and AFC99 (E). AFM 3D Surface images of AFC40 (B), AFC80 (D) and AFC99 (F)

R_{avg} and R_{rms} can be calculated by the following equations [19]:

$$R_{avg} = \frac{1}{S} \int_0^a \int_0^b |f(x, y) - z_0| dx dy \quad 1$$

Where, S , is defined as the specified area, $f(x, y)$ refers to the height in the specified area, a and b are the length of two sides of the area, and z_0 is the mean height. z_0 is given by the following:

$$z_0 = \frac{1}{S} \int_0^a \int_0^b f(x, y) dx dy \quad 2$$

$$R_{rms} = \left[\frac{1}{S} \int_0^a \int_0^b \{f(x, y) - z_0\}^2 dx dy \right]^{1/2} \quad 3$$

The roughness analysis was determined using the AFM software on the AFM images and the results are shown in Table 3. Since the RMS of all the membranes are less than 30nm, this is an indication that the surface of all the membranes is relatively smooth [27]. However, there is still a significant difference in the degree of

smoothness of each of the membranes. AFC99 is smoother than both AFC40 and AFC80 and this can be attributed to the sizes of the nodules in each membrane. Roughness reduces with increase in nodule sizes.

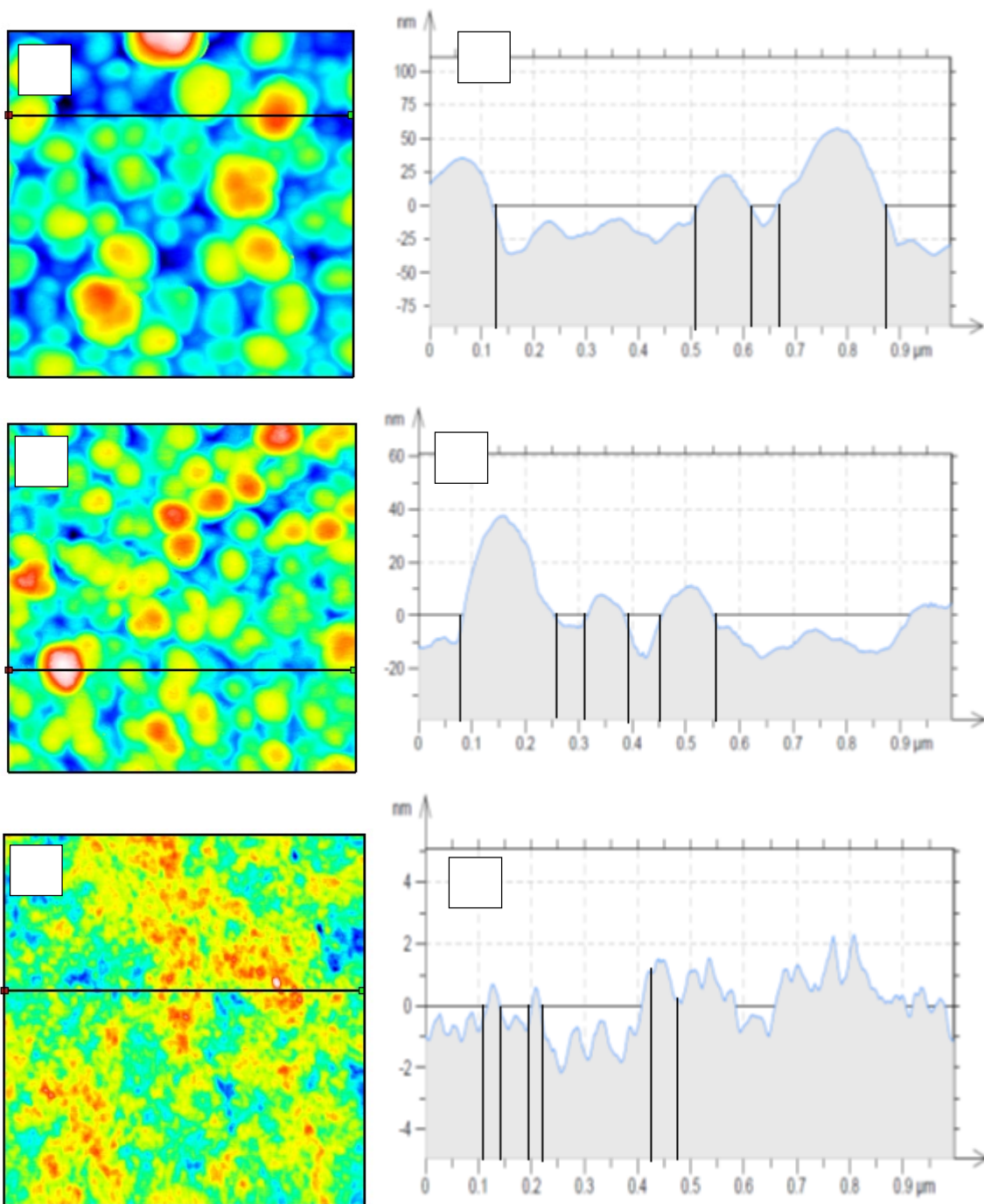


Figure 6: AFM top section analysis of AFC 40 (A&B), AFC80 (C&D), AFC99 (E&F). The nodule diameters were measured using the vertical lines drawn before and after three of the nodules. The average diameter of the nodules in AFC40 was calculated to be 130nm, while that of AFC80 and AFC99 was 120nm and 50nm respectively.

Table 3: AFM roughness analysis of AFC40, AFC80 and AFC99 using AFM software

Parameter	AFC40	AFC80	AFC99
Root mean square height (nm)	20.9	9.13	0.794
Maximum pit height (nm)	47.3	27.4	3.34
Maximum height (nm)	133	65.0	7.00
Arithmetic mean height (nm)	16.7	7.20	0.639

3.4 Pore size

The performance of membrane is affected by the pore size and the pore size distribution [4]. The pore structures such as pore size, pore size distribution, pore density, and surface roughness determines the filtration properties of the membranes. The pore structures of AFC40, AFC80 and AFC99 were examined with SEM and AFM images. The images were processed using software that includes imageJ and WSxM 5.0 Develop 8.2.

As expected, the SEM images show no visible pores. It is common to assume that reverse osmosis membranes are non-porous. Some researchers have shown evidences that the selective layers of reverse osmosis have no pore and whatever appears as pores are actually some defect on the membrane surface. This means that the membrane can be seen as homogenous structure whereby transport through it will only be by molecular diffusion [33-36]. However, it is argued that pores must be present even at molecular size otherwise no transport will occur [1]. The pores are so small, approaching molecular size, typically around the size of permeate (less than 10 Å), thus it is as if the membrane has no pore at all. The images were threshold using imageJ in order to separate the background of the image from the object. This is based on the fact that gray levels of pixels belonging to the object are substantially different from the gray levels of the pixels belonging to the background [14]. Figure 7 shows the threshold images. The threshold images revealed the pores in AFC40 and AFC80, however the pores in AFC99 are not visible. AFC99 shows no pore indicating that it is a very dense reverse osmosis membrane. AFC40 shows some pores because it is a nano filtration membrane. The properties of AFC80 are between the two.

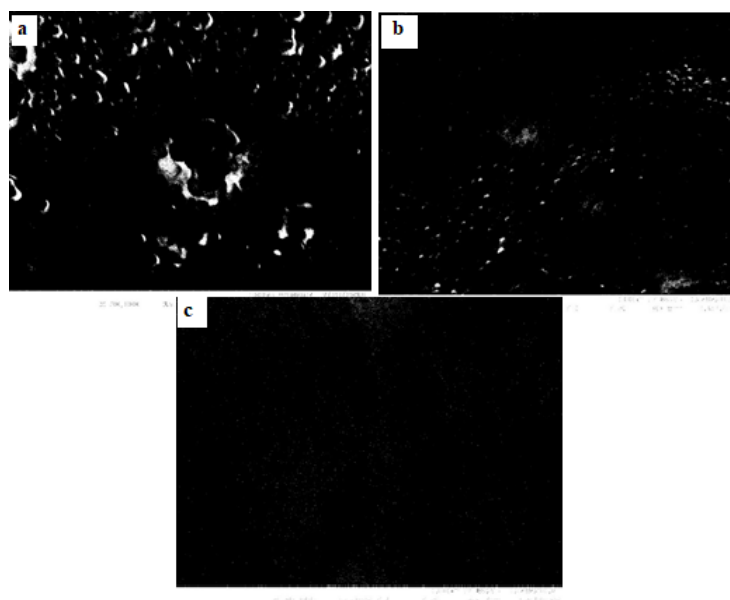


Figure 7: Threshold images of AFC40 (A), AFC80 (B) and AFC99 (C) using imageJ. AFC99 shows no pore indicating that it is a very dense reverse osmosis membrane. AFC40 shows some pores because it is a nano filtration membrane. The properties of AFC80 is between the two. [15]

3.5 Wettability

Wettability is a measure of the degree of wetting when a solid and liquid interact, and it determines whether a solid is hydrophilic or hydrophobic. The most common method of hydrophilic-hydrophobic properties of membrane is the contact angle measurement [25]. Small contact angles ($\ll 90^\circ$) indicate high wettability and characterize hydrophilic surfaces; while high contact angles ($\gg 90^\circ$) indicate low wettability and characterize hydrophobic surfaces [12]. Hydrophilic surfaces form ionic or a hydrogen bond with water molecules while hydrophobic surfaces repel water molecules. Hydrophilic-hydrophobic properties of membrane are one of the properties that determine the interaction of the membrane and foulants. These are therefore important in determining the fouling potentials of membranes [37].

Results of the contact angle measurements are shown in Figure 8 which is the average of 8 data taken for each of the membrane [38]. The results show that all the membranes have contact angles less than 90° which means

that they are all hydrophilic, however AFC40 is more hydrophilic than AFC80 and AFC99. All sodium salts are water soluble and solubility is known to have positive effect on hydrophilicity [39]. This explains why all membranes investigated which are made from organic sodium salts are hydrophilic. A lot of work is being done to modify membrane surfaces to increase its hydrophilicity [40-41]. The presence of crystalline phase of Sodium Hydrogen Sulfamate may have contributed to a higher hydrophilicity of AFC40.

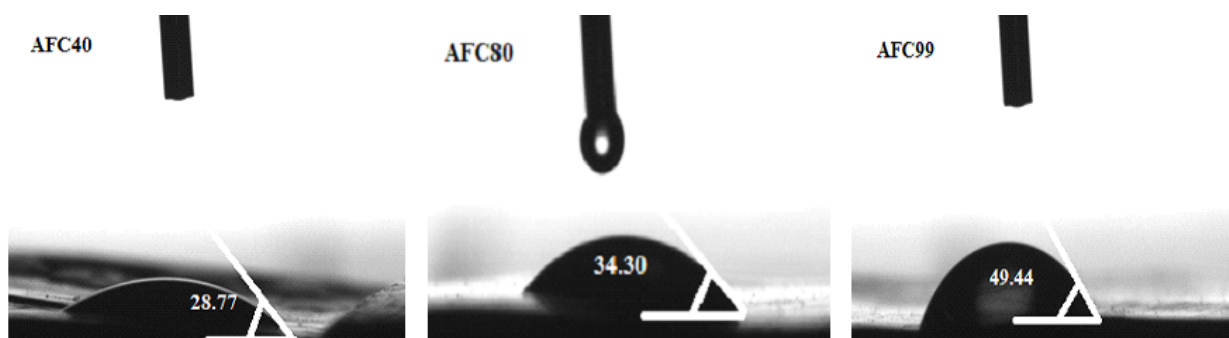


Figure 8: Contact angles for AFC40 (28.77°), AFC80 (34.30°) and AFC99 (49.44°). all the membranes have contact angles less than 90° which means that they are all hydrophilic, however AFC40 is more hydrophilic than AFC80 and AFC99.

3.6 Thermal Stability

The thermal analysis of the membrane is important to be able to predict if the membrane can handle high temperature operations that may occur in high pressure driven processes. The TGA results for the membranes are shown in Figure 9. All the membranes are thermally stable at temperature below 100°C. The analysis shows similar pattern for AFC40 and AFC99 with the material remaining stable up to 200°C and rapid degradation did not happen until a temperature of 400°C was reached, however degradation of AFC80 started at a temperature a little above 100°C. This is an indication that AFC99 and AFC40 are more thermally stable than AFC80. The reason for this is not clear. Adding sulfonate group to build polymer chains is a well-known method of introducing charge and hydrophilicity into membranes but it is also known that high degree of sulfonation can decrease the mechanical strength of membrane by causing excessive swelling [42-45].

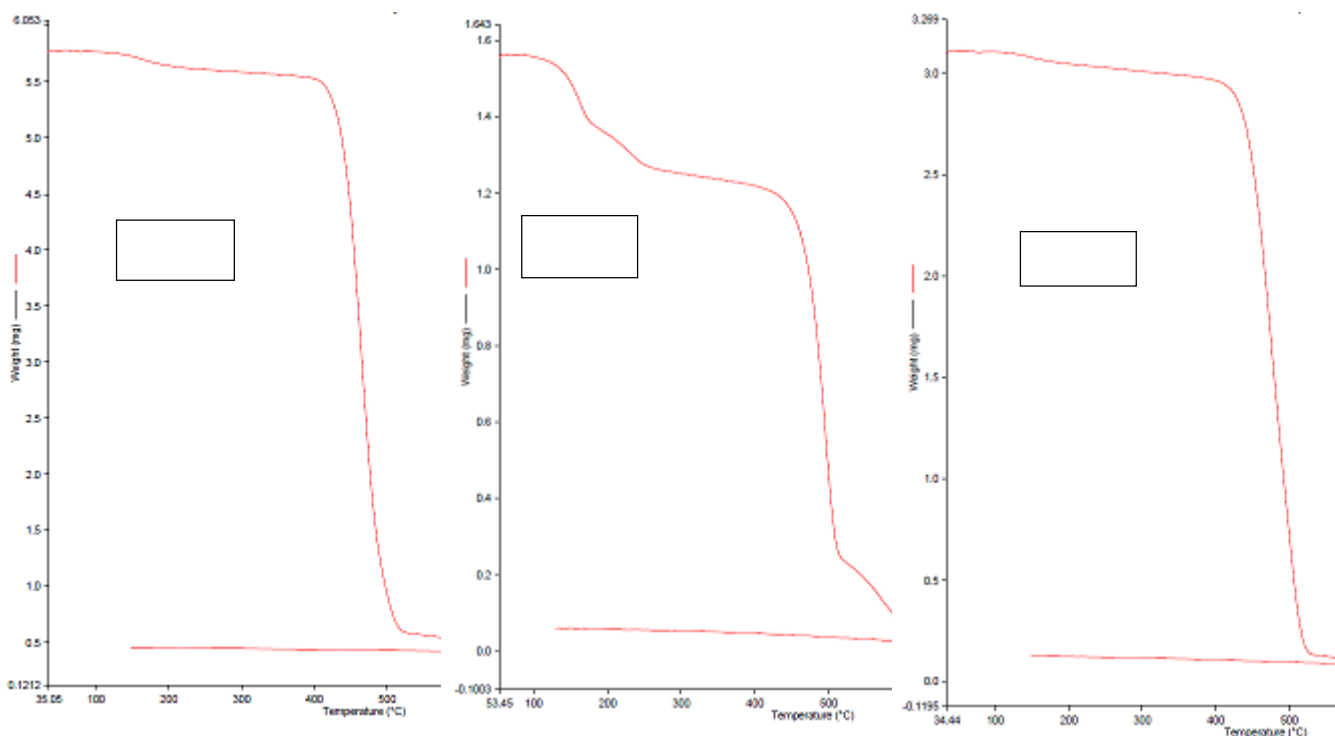


Figure 9: Thermal analysis. All the membranes are thermally stable at temperature below 100°C. The analysis shows similar pattern for AFC40 and AFC99 with the material remaining stable up to 200°C and rapid degradation did not happen until a temperature of 400°C was reached, however degradation of AFC80 started at a temperature a little above 100°C.

Conclusion

The membranes showed major differences in the nodular structure despite the fact that they were made from the same material as shown by the FT-IR and EDX results. The nodular structure was similar to that observed in a typical membrane made from polyamide that has been fabricated using interfacial polymerization. Fourier transform infrared analysis showed the functional groups at 1650 cm^{-1} which also indicated that polymerization took place during the fabrication of these membranes. The degree of polymerization was higher in AFC99 resulting in a dense membrane and less nodules sizes. The higher nodule sizes in AFC40 resulted in more rough membranes as indicated by the roughness parameter. All the membranes are hydrophilic as indicated by the contact angle which is less than 90° however AFC40 is more hydrophilic and this may also be due to higher nodule sizes and the presence of crystalline phase of Sodium Hydrogen Sulfamate. All membranes are thermally stable but the thermal stability does not seem to be influenced by the nodule sizes. It is concluded that nodule sizes are a major factor that will influence the properties and consequently may affect the performance of a membrane.

Acknowledgement-The authors would like to acknowledge National Research Foundation (NRF) of South Africa for funding and Tshwane University of Technology for the use of Laboratory facilities.

References

1. S.J. Zaidi, F. Fadhillah, Z. Khan, A.F. Ismail, *Desalination*. 368 (2015) 202-213.
2. C. Bellona, J.E. Drewes, P. Xu, G. Amy, *Water Research*. 38, 12 (2004) 2795-2809.
3. B.S. Lalia, V. Kochkodan, R. Hashaikheh, N. Hilal, *Desalination*. 326 (2013) 77-95.
4. K.C. Khulbe, C.Y. Feng, T. Matsuura, Springer Science & Business Media. (2007).
5. M.N. Hegde, A. Moany, *Journal of Conservative Dentistry: JCD*. 15, 1 (2012) 61.
6. J.E. Welton, *SEM Petrology Atlas* (1984): 237.
7. Y. Wyart, G. Georges, C. Deumie, C. Amra, P. Moulin, *Journal of Membrane Science*. 315, 1-2 (2008) 82-92.
8. W.R. Bowen, N. Hilal, Butterworth-Heinemann. Atomic force microscopy in process engineering an introduction to afm for improved processes and pro ISBN-13:978-1-85617-517-3(2009).
9. A. Cassetta, *Encyclopedia of Membranes*. (2015) 1-3.DOI 10.1007/978-3-642-40872-4_1102-2
10. R.M. Silverstein, F.X. Webster, D.J. Kiemle, D.L. Bryce, *Spectrometric Identification of Organic Compounds*, ISBN: 978-0-470-61637-6(2014).
11. P. Gabbott, *Principles and Applications of Thermal Analysis* ed. John Wiley & Sons. ISBN-13:978-1-4051-3171-1(2008).
12. Y. Yuan, T.R. Lee, In *Surface Science Techniques*.3-34. Springer, Berlin, Heidelberg, ISBN :978-3-642-34242-4 (2013).
13. I. Horcas, R. Fernández, J. M. Gomez-Rodriguez, J. W. S. X. Colchero, J. W. S. X. M. Gómez-Herrero, A. M. Baro, *Review of Scientific Instruments*. 78, 1 (2007) 013705.
14. J. Broeke, J.M.M. Pérez, J. Pascau, *Image Processing with ImageJ*, PacktPublishing Ltd. ISBN :978-1-75388-983-7(2015).
15. A. Adeniyi, R. Mbaya, M. Onyango, P. Popoola, T. Brooms, *WIT Transactions on Ecology and the Environment*. 223 (2017) 583-592.
16. B.S. Mbuli, E.N. Nxumalo, S.D. Mhlanga, R.W. Krause, V.L. Pillay, Y. Oren, C. Linder, B.B. Mamba, *Journal of Applied Polymer Science* 131, 8 (2014).
17. S.H. Son, J. Jegal, *Journal of applied polymer science*. 120, 3 (2011) 1245-1252.
18. A.C. Sagle, E.M. Van Wagner, H. Ju, B.D. McCloskey, B.D. Freeman, M.M. Sharma, *Journal of Membrane Science*. 340, 1-2 (2009) 92-108.
19. S., Al-Jeshi, A. Neville, *Desalination*. 189, 1-3 (2006) 221-228.

20. D. Emadzadeh, W. J. Lau, M. Rahbari-Sisakht, A. Daneshfar, M. Ghanbari, A. Mayahi, T. Matsuura, A. F. Ismail, *Desalination*. 368 (2015) 106-113.
21. A.K. Ghosh, E.M.V. Hoek, *Journal of Membrane Science*. 336, 1-2 (2009) 140-148.
22. L. Bai, Y. Liu, N. Bossa, A. Ding, N. Ren, G. Li, H. Liang, M.R. Wiesner, *Environmental Science & Technology*. 52, (2018) 11178-11187.
23. I. Pinnau, B.D. Freeman, *Membrane Formation and Modification*. 744 (2000) 1-22.
24. F. Liu, N.A. Hashim, Y. Liu, M.R.M. Abed, K. Li, *Journal of Membrane Science*. 375, 1-2 (2011) 1-27.
25. B.J.A. Tarboush, D. Rana, T. Matsuura, H.A. Arafat, R. M. Narbaitz, *Journal of Membrane Science*. 325, 1 (2008) 166-175.
26. V Kochkodan, N Hilal, *Desalination*. 356 (2015) 187-207.
27. S. Yu, M. Liu, Z. Lü, Y. Zhou, C. Gao, *Journal of Membrane Science*. 344, 1-2 (2009) 155-164.
28. I. M. Wienk, R. M. Boom, M. A. M. Beerlage, A. M. W. Bulte, C. A. Smolders, H. Strathmann, *Journal of Membrane Science*. 113, 2 (1996) 361-371.
29. D. M. Koenhen, M. H. V. Mulder, C. A. Smolders, *Journal of Applied Polymer Science*. 21, 1 (1977) 199-215.
30. C. Lee, S. Sundar, J. Kwon, H. Han, *Journal of Polymer Science Part A: Polymer Chemistry*. 42, 14 (2004) 3621-3630.
31. E.M.V. Hoek, S. Bhattacharjee, M. Elimelech, *Langmuir*. 19, 11 (2003) 4836-4847.
32. W.R. Bowen, T.A. Doneva. *Journal of Colloid and Interface Science*. 229, 2 (2000) 544-549.
33. S. Rosenbaum, O. Cotton, *Journal of Polymer Science Part A- 1: Polymer Chemistry*, 7, 1 (1969) 101-109.
34. C. Fritzmann, J. Löwenberg, T. Wintgens, T. Melin, *Desalination*, 216, 1-3 (2007) 1-76.
35. M. Wilf, K. Klinko, *Desalination* 173, 1 (2005) 1-12.
36. K.A. Mauritz, R.B. Moore, *Chemical Reviews*. 104, 10 (2004) 4535-4586.
37. V. Kochkodan, D.J. Johnson, N. Hilal, *Advances in Colloid and Interface Science*, 206, 116-140.
38. T. Zhang, C. Zhu, H. Ma, R. Li, B. Dong, Y. Liu, S. Li, *Journal of Membrane Science*. 457 (2014) 88-94.
39. D. Mackay, A. Bobra, W.Y. Shiu, S.H. Yalkowsky. *Chemosphere*. 9, 11 (1980) 701-711.
40. J.T. Arena, B. McCloskey, B.D. Freeman, J.R. McCutcheon, *Journal of Membrane Science*. 375, 1-2 (2011) 55-62.
41. G. Han, S. Zhang, X. Li, N. Widjojo, T.S. Chung, *Chemical Engineering Science*. 80 (2012) 219-231.
42. M. Ulbricht, *Polymer*. 47, 7 (2006) 2217-2262.
43. H. Ju, B.D. McCloskey, A.C. Sagle, Y.H. Wu, V. A. Kusuma, B. D. Freeman, *Journal of Membrane Science*. 307, 2 (2008) 260-267.
44. H.B. Park, B.D. Freeman, Z.B. Zhang, M. Sankir, J. E. McGrath, *Angewandte Chemie International Edition*. 47, 32 (2008) 6019-6024.
45. M. Paul, H.B. Park, B.D. Freeman, A. Roy, J.E. McGrath, J. S. Riffle, *Polymer*. 49, 9 (2008) 2243-2252.

(2019) ; <http://www.jmaterenvirosci.com>